Electronic structure and stability of the pentlandites Co_9S_8 and $(Fe,Ni)_9S_8$

H. R. Chauke,[1] D. Nguyen-Manh,[2] P. E. Ngoepe,[1,3] D. G. Pettifor,[2] and S. G. Fries[4]
[1]*Materials Modeling Center, University of the North, Private Bag x1106, Sovenga 0727, South Africa*
[2]*Department of Materials, University of Oxford, OX1 3PH Oxford, United Kingdom*
[3]*Manufacturing and Materials Technology, Council for the Scientific and Industrial Research, P.O. Box 395, Pretoria 0001, South Africa*
[4]*ACCESS e.V., RWTH Aachen, Intzestrasse 5, D-52072 Aachen, Germany*
(Received 12 March 2002; revised manuscript received 23 June 2002; published 14 October 2002)

First-principle electronic structure investigations of transition-metal sulfides Co_9S_8 and related alloys with the unique structure of pentlandite are carried out using density-functional theory within the local-density approximation. The total-energy calculations for Co_9S_8 and $(Fe,Ni)_9S_8$ alloys have been computed and we predict equilibrium lattice parameters that are on average 1% smaller than in the experiment. The heats of formation have been calculated, the theoretical prediction for Co_9S_8 being in excellent agreement with that available in the Thermocalc database. The predicted heat of formation for the $Fe_5Ni_4S_8$ alloy is very close to Co_9S_8, reflecting the fact that the Fermi level is found to fall in a pseudogap for an average number of valence electrons per atom $e/a=7.58$. Furthermore, we determined the individual bond energies for Co_9S_8 and Co_8S_8 to stress the contribution of the octahedral metal cobalt to the stability of the Co_9S_8 phase.

DOI: 10.1103/PhysRevB.66.155105 PACS number(s): 31.15.Ar, 31.15.Ew, 07.05.Tp, 07.05.−t

I. INTRODUCTION

Transition-metal sulfides are a major group of minerals that provide the crystal chemist with a number of diverse structural types to study. Among these, the pentlandite structure is taken by sulfides with chemical formulas that do not usually display normal chemical valence, such as in the case of the only known binary phase of pentlandite, Co_9S_8.[1] The structure of the pentlandites $(Fe,Ni)_9S_8$ and Co_9S_8 was determined by Lindqvist *et al.*[2] by means of powder diffraction. This structure was confirmed subsequently by Pearson and Buerger[3]and Geller[4] with single-crystal methods. The structure of Co_9S_8 has been refined in the space group $Fm3m$ (225) and the primitive unit cells of Co_9S_8 and Co_8S_8 are shown in Fig. 1, and the crystal atomic positions are presented in Table I. There are four Co_9S_8 units in the conventional cubic unit cell, with the sulfur atoms forming an almost cubic close-packed framework. Two nonequivalent metallic sites are present in the unit cell, the one represented by the four octahedral sites, $M(O)$, the other by the 32 tetrahedral sites, $M(T)$.[5] The primitive unit cell consists of 17 atoms with one octahedral metal atom $M(O)$, eight tetrahedral metal atoms $M(T)$, two linking sulfurs S(l) and six face-capping sulfurs S(f) atoms.

The electronic density of states for Co_9S_8 has been calculated using *ab initio* density-functional methods within the generalized gradient approximation (GGA). It has been stressed that the stability of Co_9S_8 phase results mainly from the formation of the structure-induced pseudogap at the Fermi energy.[6] The electronic structure of the polyhedral clusters in Co_9S_8 has been analyzed using the extended Hückel calculations.[1] In particular, it has been stressed that the metal-metal bonding effects confined to the cube cluster are found to be severely affected by through-bond coupling with their nearest-neighboring sulfide atoms. On the other hand, the crucial role played by the strong d-p hybridization in the formation of the semiconductor band gaps in different transition- and precious-metal sulfides has been emphasized in recent first-principle calculations.[7,8]

The purpose of this paper is to perform a systematic study of the electronic structure in order to clarify the relationship between the shape of the electronic density of states (DOS) and the structural stability of Co_9S_8 and related alloys. We have performed total-energy minimization with respect to the volume keeping the two internal coordinates of the pentlandite structure fixed. The heat of formation as a function of average valence electron per atom for M_9S_8, M_8S_8, and $(M,N)_9S_8$ alloys, together with their corresponding cohesive energies, have been calculated. We have found that the high stability of Co_9S_8 and $Fe_5Ni_4S_8$ phases is correlated with their Fermi levels falling in a pseudogap corresponding to an average number of electrons per atom, $e/a=7.58$. We have calculated the individual bond energies for both Co_9S_8 and Co_8S_8 in order to stress the important contribution of the octahedral metal cobalt to the stability of the Co_9S_8 phase.

The outline of this paper is as follows. The computational details are described in Sec. II. The calculated electronic density of states and predicted heats of formation are presented in Sec. III. The relative stability of Co_9S_8 versus Co_8S_8 is discussed in Sec. IV. We conclude in Sec. V.

II. COMPUTATIONAL DETAILS

The electronic structure and the total energy have been calculated self-consistently using the Tight-binding linear-muffin-tin-orbital (TB-LMTO) technique within the atomic-sphere approximation with combined correction (ASA + CC).[9] Exchange and correlation were included using the von Barth–Hedin formula within the local-density-functional description.[10] In the ASA+CC, the one-electron potential entering the Schrödinger equation is a superposition of overlapping spherical potential wells with position **R** and radius $s_{\mathbf{R}}$, which leads to a kinetic-energy error that is proportional

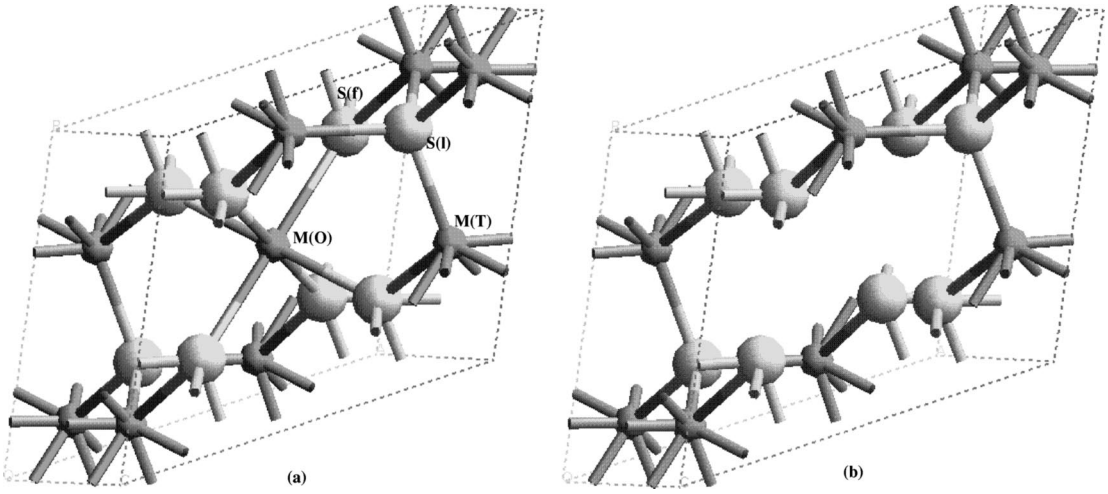

FIG. 1. Crystal structure of pentlandite: The primitive unit cell of (a) Co_9S_8 and (b) Co_8S_8. $M(O)$, octahedral metal; $M(T)$, tetrahedral metal; S(l), linking sulfurs; S(f), face-capping sulfurs.

to the fourth power of the relative sphere overlap $\omega_{\mathbf{RR}'}$,[11] where

$$\omega_{\mathbf{RR}'} \equiv \frac{s_{\mathbf{R}} + s_{\mathbf{R}'}}{|\mathbf{R} - \mathbf{R}'|} - 1. \tag{1}$$

In many mineral structure types such as the pentlandites, the use of only atom-centered spheres within ASA would cause substantial error, either due to large overlap and misrepresentation of the potential, or due to neglect of charge in the van der Waals gap. Therefore, it is necessary to pack the van der Waals gap with interstitial spheres. In general, the requirement for choosing the sphere positions and radii is that the superposition of the spherical potentials approximates the full three-dimensional potential as accurately as possible, so that the overlap error for the kinetic energy remains acceptable. Here, following Ref. 11, the full potential is first represented by the superposition of neutral-atom Hartree potentials. The atomic-centered spheres are then determined by tracing the potential along the lines connecting nearest-neighbor atoms and finding the saddle points. For a given atom with position **R**, the distance to the closest saddle point is taken as the radius of its sphere and usually touches the sphere constructed in the same way from the other atom. The ASA radii are then obtained by inflating these atom-centered nonoverlapping spheres until they either fill space or until their overlap $\omega_{\mathbf{RR}'}$ reaches a maximum of 16%. In the latter case, the potential between the atomic potentials must be represented by additional interstitial spheres, which are usually repulsive. The positions of these interstitial spheres are chosen among the nonoccupied symmetry positions of the space group. Then their radii are chosen in such a way that the maximum overlap between an atomic and an interstitial sphere is 18% and the maximum overlap between two interstitial spheres is 20%. This procedure is automated in the computer program.[9]

The above procedure leads to one $I1$, six $I2$ and eight $I3$, new interstitial sphere symmetry positions per unit cell for Co_9S_8. The interstitial spheres $I1$, $I2$, and $I3$ occupy the sites $4a(0,0,0)$, $8c(1/4,1/4,1/4)$, and $32f(-0.369,-0.369,-0.369)$, respectively. For the case of $(Fe,Ni)_9S_8$, the interstitial spheres are labeled $I1$ to $I15$ since their sphere radii differ significantly due to the Fe/Ni distribution over the octahedral and the tetrahedral sites. The basis set consisted of (Fe,Co,Ni) $4s$, $4p$, $3d$; S $3s$, $3p$, $3d$ and interstitial spheres $I\,2s$, $3p$, $4d$. All **k** space integrations were performed by the tetrahedron method. Convergence to self-consistency was achieved with the use of $4\times4\times4$ number of **k** points in the irreducible zone that leads to a precision of 10^{-5} Ry/f.u.. The experimental internal parameters for Co_9S_8 have been kept fixed during our calculations, allowing only the lattice parameter a_0 to vary, thereby minimizing the total energy with respect to volume. We have used the same internal co-

TABLE I. Crystal structure positions of pentlandite $(Co,Fe,Ni)_9S_8$ Co(O) and Co(T) denote the octhedral $M(O)$ and tetrahedral $M(T)$, respectively. Co/Fe/Ni entered as Co.

Atoms	Positions	x	y	z
Co(O)	($4b$)	0.5000	0.5000	0.5000
Co(T)	($32f$)	0.1261	0.1261	0.1261
S(l)	($8c$)	0.2500	0.2500	0.2500
S(f)	($24e$)	0.2629	0.0000	0.0000

TABLE II. The predicted equilibrium lattice parameter (a_{eq}), equilibrium volume (V_{eq}), binding energy (E), and bulk modulus (B) for Co_9S_8 and $(Fe,Ni)_9S_8$. The experimental values are in parenthesis, Ref. 2.

Materials	a_{eq} (Å)	V_{eq} (Å^3/atom)	E (eV/atom)	B (GPa)
Co_9S_8	9.918 (9.928)	14.33	−5.968	152.8
Fe_9S_8	9.948	14.46	−5.290	152.3
Ni_9S_8	10.118	15.21	−5.131	122.7
$Fe_5Ni_4S_8$	9.938 (10.128)	14.42	−5.327	149.5
$Fe_4Ni_5S_8$	9.991 (10.100)	14.64	−5.262	140.7

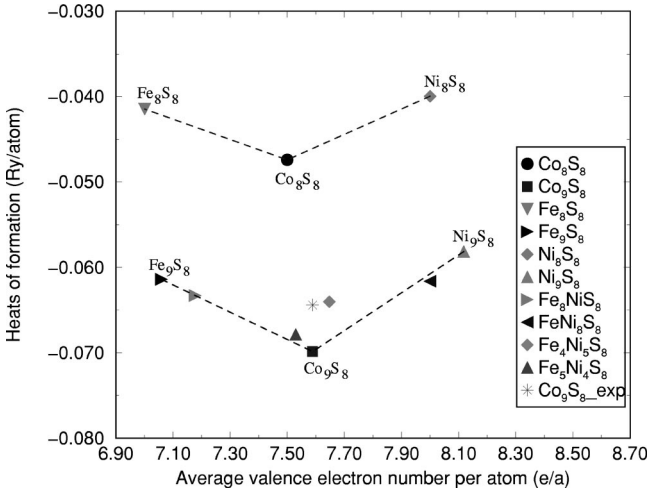

FIG. 2. Heats of formation (ΔH_f) for $(Fe,Co,Ni)_9S_8$ alloys as a function of the average number of valence electrons per atom (e/a) together with the M_8S_8 stoichiometry. The dashed lines connecting the binary values for the 9:8 and 8:8 stoichiometries are drawn to aid the eye. The single experimental value for Co_9S_8 is taken from the Thermocalc database, Ref. 13.

ordinates for $(Fe,Ni)_9S_8$. Self-consistency was deemed to have been achieved at 10^{-2} mRy per unit cell.

III. HEATS OF FORMATION

The heat of formation may be calculated by subtracting the binding energies of the elemental systems from that of the compound. Hence, the heat of formation per atom of pentlandite $(M,N)_9S_8$ is given by

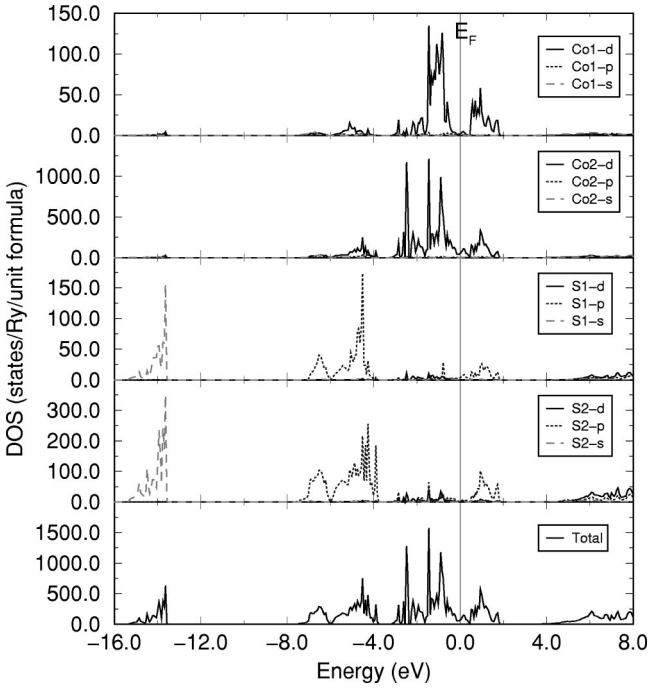

FIG. 3. Total, local, and partial density of states of Co_9S_8, where the Fermi energy is taken as the zero of energy. Co1, Co2, S1, and S2 represent Co(O), Co(T), S(l) and S(f), respectively.

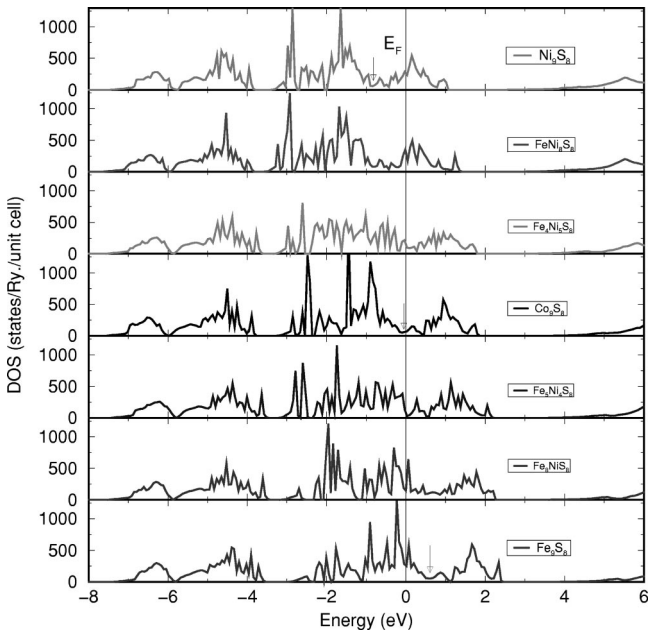

FIG. 4. Total density of states for Co_9S_8 and related alloys $[(Fe,Ni)_9S_8]$, where the Fermi energy is taken as the zero of energy. The arrows show the position of the pseudogap with respect to the Fermi energy.

$$\Delta H_f[(M,N)_9S_8] \equiv \Delta H_f(M_xN_{9-x}S_8) = 1/17[E(M_xN_{9-x}S_8) - xE(M) - (9-x)E(N) - 8E(S)], \quad (2)$$

where M, N are chosen from Co, Fe, or Ni. The energies of the elemental transition metal systems Co,Fe, and Ni were evaluated in the magnetic spin-polarized state in hcp, bcc, and fcc structures, respectively, whilst elemental S was calculated using the experimental ground-state structure.[12] The predicted equilibrium lattice constants a_{eq}, atomic volume V_{eq}, binding energy E, and bulk modulus B are given in Table II. The binding energies are measured relative to the free atomic state values calculated assuming Co d^8s, Fe d^7s, Ni d^9s, and S s^2p^4. We see that the predicted lattice constants are in good agreement with experiment for those alloys found experimentally, the largest error being 2% for $Fe_5Ni_4S_8$. We furthermore observe that Co_9S_8 has the strongest binding energy and largest bulk modulus, which correspond to its smallest equilibrium atomic volume.

The heat of formation for $(Co, Ni, Fe)_9S_8$ alloys as a function of the average number of valence electrons per atom (e/a) is shown in Fig. 2, together with M_8S_8 in which the octahedral metal atoms have been removed. We see that the only available experimental value, namely, that for Co_9S_8 from the thermocalc database (CALPHAD),[13] agrees very well with our prediction. It is clear from this figure that Co_9S_8 has the largest heat of formation as compared to the other phases. This indicates highest stability for the Co_9S_8 stoichiometry. Interestingly, the heats of formation of $Fe_5Ni_4S_8$ and $Fe_4Ni_5S_8$ lie very close to this minimum as expected from their occurrence in nature. However, Fe_9S_8 and Ni_9S_8 on the other hand, fall on the upper portion of the plot indicating

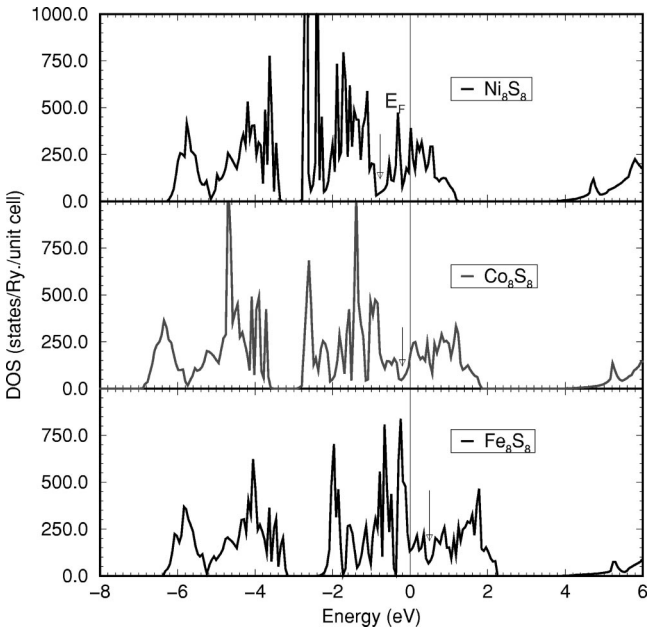

FIG. 5. Total density of states for Fe_8S_8, Co_8S_8, and Ni_8S_8 where the Fermi energy is taken as the zero of energy. The arrows show the position of the pseudogap with respect to the Fermi energy.

that they may be unstable pentlandite phases. Furthermore, it is shown clearly that the M_8S_8 framework has a much reduced heat of formation, thereby demonstrating the loss of stability compared to the M_9S_8 stoichiometry.

The V-shaped trend in both the 9:8 and 8:8 curves in Fig. 2 can be understood from the behavior of the corresponding DOS, which are plotted in Figs. 3–5. We first consider the partial s,p, and d DOS for Co_9S_8 in Fig. 3. Our TB-LMTO DOS are very similar to those calculated previously by the plane-wave Vienna *ab initio* simulation program (VASP).[6] In particular, we see that the octahedral Co sites have their d band split into the filled t_{2g} levels and unfilled antibonding e_g levels, as discussed in detail elsewhere.[1] We find that the total DOS shows a small pseudogap opening up at the Fermi energy. The change in the position of this pseudogap with respect to the Fermi energy across the pentlandites from Fe_9S_8 to Ni_9S_8 is illustrated in Fig. 4. We can now understand the V-shaped behavior in the 9:8 heats of formation. As the number of electrons per atom increases, initially additional bonding states are occupied until the Fermi energy reaches the middle of the pseudogap around $e/a=7.58$, whereafter the antibonding states are filled. Hence, we observe the V-shaped behavior of ΔH_f from Fe_9S_8 through Co_9S_8 to Ni_9S_8. The 8:8 phases also show the same V-shaped behavior, because their DOS in Fig. 5 display a similar pseudogap around $e/a=7.31$. We examine, however, the loss in stability of nearly 0.3 eV per atom in going from the 9:8 to 8:8 phases in the following section.

IV. STABILITY OF Co_9S_8 VERSUS Co_8S_8

In this section we explore the stability of the 9:8 stoichiometry versus the equiatomic 8:8 stoichiometric sulfide, which we see from Fig. 2 has a 35% smaller heat of formation. Table III compares the individual bond energies of the two different stoichiometries where the bond energy between atoms i and j is defined by

$$E_{bond}^{ij}=2Tr\beta_{ij}\Theta_{ji}, \tag{3}$$

where the trace runs over the different atomic orbitals on the two sites. β_{ij} and Θ_{ji}, represent the bond integral and bond order matrices, respectively. To clarify the importance of the octahedral coordinated metal atom (Co) to the stability of the Co_9S_8 stoichiometry, we compare the individual bond energies between Co_9S_8 and Co_8S_8. The bond energies and bond distances are shown in Table III. The bond energy varies depending on the number of nearest-neighbor atoms and the distance between the individual atoms. The bond distances for Co_8S_8, which are obtained by relaxing the structure using the plane-wave CASTEP code,[14] show values similar to Co_9S_8. As expected, there is no bonding between the octahedral metal, Co(O) and sulfur, S(f), because the octahedral coordinated metal atoms Co(O) have been removed in the Co_8S_8 framework, whereas the bond energy is large for

TABLE III. Bond energies for Co_9S_8 and Co_8S_8.

		Co_9S_8		Co_8S_8		
Bond	No. of bonds	d(Å)	E_b (Ry/bond)	d(Å)	E_b (Ry/bond)	ΔE_b
Co(O)-S(f)	6	2.389	−0.17838			0.17838
Co(T)-S(l)	1	2.130	−0.31639	2.132	−0.31635	0.00004
Co(T)-S(f)	3	2.206	−0.24522	2.208	−0.24498	0.00024
Co(T)-Co(T)	3	2.499	−0.06368	2.502	−0.06308	0.00060
Co(T)-Co(T)	6	3.478	−0.00067	3.482	−0.00057	0.00010
S(l)-Co(T)	4	2.130	−0.31639	2.132	−0.31635	0.00040
S(l)-S(f)	12	3.508	0.00163	3.511	0.00182	0.00019
S(f)-Co(T)	4	2.206	−0.24522	2.208	−0.24498	0.00024
S(f)-Co(O)	1	2.389	−0.17838			0.17838
S(f)-S(f)	4	3.379	0.00364	3.382	0.00337	0.00027
S(f)-S(f)	4	3.634	−0.00075	3.638	−0.00117	0.00042
S(f)-S(l)	4	3.508	0.00163	3.511	0.00181	0.00018

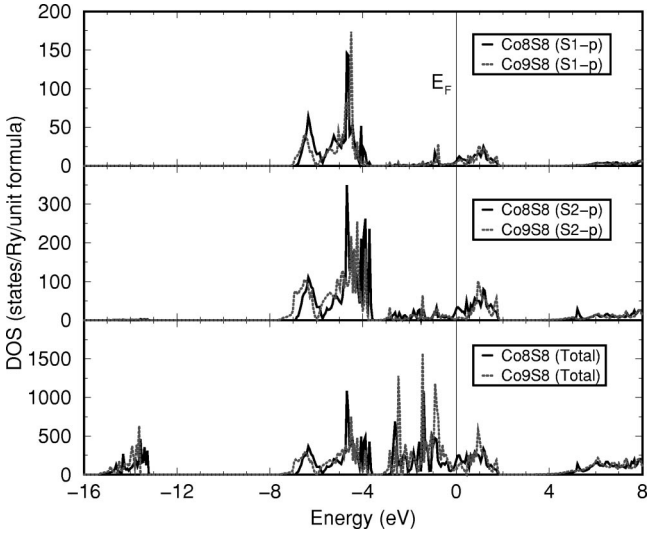

FIG. 6. Total and partial density of states for Co_9S_8 and Co_8S_8, where the Fermi energy is taken as the zero of energy.

Co_9S_8 (-0.178 Ry/bond). We note that the shorter bond length corresponds to a stronger bond with more negative bond energy. We further observe strong bonding between the tetrahedral metal Co(T) and sulfur S(l) that corresponds to the short bond length of 2.130 Å and 2.132 Å for Co_9S_8 and Co_8S_8, respectively. Most interestingly the bond energy between the nearest-neighbor atoms for both systems shows a negligible change of only about 0.0001 Ry/bond on average. Therefore, we have demostrated that the stability of the Co_9S_8 compared to Co_8S_8 framework is driven by the bond Co(O)-S(f) in Co_9S_8 which is absent in Co_8S_8, the other bonds being affected to a much lesser extent.

The total and partial densities of states for Co_9S_8 and Co_8S_8 are compared in Fig. 6. It is clear from the total density of states that the Fermi energy on Co_8S_8 stoichiometry does not fall in the middle of the pseudogap. The partial densities of states were computed for the $3p$ orbitals of sulfur S(l) and S(f) to show the contribution from the bonding between the $3p$ orbital of sulfur and the cobalt $3d$ orbitals. There is no difference in the p-orbital projection of sulfur S(l), so that S(l) does not change its state of bonding between Co_9S_8 and Co_8S_8. However, the p-orbital projections for the sulfurs S(f) are different. We observe a large peak at lower energy of ≈ -4.8 eV on the Co_8S_8 projection which is lacking in the Co_9S_8 phase. This peak corresponds entirely to the nonbonding p_z orbital of S(f). In the energy range between -6.04 and -7.5 eV, we note that the orbitals are separated by a shift of approximately 0.4 eV. This energy shift compares very well with the predicted heat of formation discussed above. We believe that this energy shift depends entirely on the bonding between the octahedral Co(O) $3d$ and S(f) $3p$ orbitals which is lacking in the Co_8S_8 stoichiometry.

V. CONCLUSION

We have used the TB-LMTO method to examine the stability of the transition-metal sulfides with pentlandite structure. In particular, we have predicted the heats of formation of Co_9S_8 and $(Fe,Ni)_9S_8$ alloys, finding that Co_9S_8 displays the largest heat of formation with a value of -91.5 kJ/mole that is in close agreement with the -85.1 kJ/mole from the Thermocalc database. This strong stability of Co_9S_8, and also $Fe_5Ni_4S_8$, is correlated with their Fermi levels lying within a pseudogap that separates the bonding from antibonding states. Finally, the critical importance of the octahedral cobalt sites in stabilizing the 9:8 stoichiometry is demonstrated by comparing the individual bond energies of the pentlandites with the hypothetical 8:8 phase in which the octahedral sites are removed.

ACKNOWLEDGMENTS

This work was supported by the Royal Society-National Research Foundation collaboration between the University of the North in South Africa and certain universities in the United Kingdom. Computations were performed in the Materials Modeling Center, University of the North and the Materials Modeling Laboratory, Department of Materials, Oxford University.

[1] J.K. Burdett and G.J. Miller, J. Am. Chem. Soc. **109**, 4081 (1987).
[2] M. Lindqvist, D. Lindqvist, and A. Westgren, Svensk Kem. Tidsk **48**, 156 (1936).
[3] A.D. Pearson and M.J. Buerger, Am. Mineral. **41**, 804 (1956).
[4] S. Geller, Acta Crystallogr. **15**, 1195 (1962).
[5] Tatsuhiro Tsukimura and Hiromoto Nakazawa, Acta Crystallogr., Sect. B: Struct. Sci. **40**, 364 (1984).
[6] P. Raybaud, J. Hafner, G. Kresse, and H. Toulhoat, J. Phys.: Condens. Matter **9**, 11 107 (1997).
[7] D. Nguyen-Manh *et al.*, in *Tight-Binding Approach to Computational Material Science*, edited by P.E.A. Turchi, MRS Symposia Proceedings No. 491 (Materials Research Society, Pittsburgh, 1998) p. 401.
[8] D. Nguyen-Manh, P.S. Ntoahae, D.G. Pettifor, and P.E. Ngoepe, Mol. Simul. **22**, 1 (1999).
[9] G. Krier, O. Jepsen, A. Burkhart, and O.K. Andersen, TB-LMTO-ASA program, Stuttgart, April 1995.
[10] U. von Barth and L. Hedin, J. Phys. C **5**, 1629 (1972).
[11] O.K. Andersen, O. Jepsen, and G. Krier, in *Method of Electronic Structure Calculations*, edited by V. Kumar, O. K. Anderson, and A. Mookerjee (World Scientific, Singapore, 1994).
[12] P. Villars and L.D. Calvin, *Pearson's Handbook of Crystalographic Data for Intermetallic Phases* (American Society for Metals, Metals Park, OH, 1985), Vol. 1–3.
[13] S.G. Fries *et al.* (unpublished).
[14] CERIUS 3.0. Quantum Mechanics-Physics. CASTEP, ESOCS, Fast Structure, April 1997, MSI, San Diego, CA.